Supplementary Materials

Table S1. Summary of data information used in this study.

Data Types	Unit	Source	Accuracy
CO_2 concentration	ppm	ABB greenhouse gas analyzer output	0.35 ppm
Temperature	℃	ERA5 reanalysis data	—
Pressure	hPa	ERA5 reanalysis data	—
Wind speed	m/s	ERA5 reanalysis data	—
Wind direction	°	Derived from ERA5 U/V components	—

Table S2. Carbon Emission Conversion Factors for Fossil Fuels [1].

Fuel Type	Net Calorific Value (tC/TJ)	Unit Carbon Content per Energy (TJ/10,000t, except for natural gas which is expressed as TJ/100 million m^3)	Carbon Oxidation Rate (%)
Other Washed Coal	25.41	105.54	90
Coke	29.50	284.35	93
Kerosene	19.60	430.70	98
Liquefied Petroleum Gas	17.20	501.79	99
Natural Gas	15.32	3893.1	99
Fuel Oil	20.08	418.16	98
Diesel	20.20	433.30	98
Raw Coal	15.30	293.07	93
Gasoline	18.90	448.00	98
Crude Oil	20.08	418.16	98
Liquefied Natural Gas	15.30	418.68	99

Based on the **Table S2**, the carbon emissions from different fossil fuels were estimated using key parameters, including the Net Calorific Value (tC/TJ), Unit Carbon Content per Energy, and Carbon Oxidation Rate (%). The unit carbon content per energy represents the carbon emissions per unit of energy released during combustion. For solid and liquid fuels, the unit is expressed as TJ/10,000 t, whereas for natural gas, it is given in TJ/100 million m^3 to reflect their volumetric nature.

The carbon emissions were calculated following the standard emission estimation approach:

$$E_{CO_2} = AD \times EF \times 44/12$$

$$AD = a \times UC$$

$$EF = NCV \times OR$$

Where: E_{CO2} represents the total CO_2 emissions, AD (Activity Data) represents fuel consumption amount in TJ, a represents the fuel consumption amount in either 10,000 t for

solid and liquid fuels or 100 million m3 for natural gas, UC (Unit Carbon Content per Energy) corresponds to the emission factor for each fuel type, EF (Emission Factor) is determined by the Net Calorific Value (NCV, tC/TJ) multiplied by the Carbon Oxidation Rate (OR, %).

Table S3. Energy activity levels from the industrial sector in Chengdu, as reported in the Chengdu Statistical Yearbook from 2010 to 2022.

Year \ Fuel Type	Other Washed Coal (10,000 t)	Coke (10,000 t)	Kerosene (10,000 t)	Liquefied Petroleum Gas (10,000 t)	Natural Gas (100 million m^3)	Fuel Oil (10,000 t)	Diesel (10,000 t)	Raw Coal (10,000 t)	Gasoline (10,000 t)	Crude Oil (10,000 t)	Liquefied Natural Gas (10,000 t)
2010	37.89	113.84	2.23	0.04	26.50	0.18	6.69	632.52	4.13	342.84	0.00
2011	21.60	101.49	2.00	0.04	28.60	9.52	6.91	785.15	4.08	347.94	0.00
2012	20.00	93.57	1.92	0.04	24.33	0.16	6.26	658.39	3.88	575.14	0.00
2013	19.76	80.31	1.75	0.04	28.85	0.09	5.93	571.41	3.35	435.67	0.00
2014	8.38	72.15	0.08	0.21	27.35	5.76	5.44	491.32	2.96	457.90	0.00
2015	6.50	7.40	0.86	16.38	24.94	10.46	5.18	415.17	3.05	431.59	0.00
2016	10.53	4.38	1.04	19.92	26.48	11.39	5.49	402.35	3.17	506.73	0.00
2017	7.43	1.01	0.07	17.75	26.95	12.40	5.22	384.81	2.76	559.16	0.00
2018	0.88	1.39	0.08	15.94	25.97	9.46	4.59	349.90	2.24	699.94	0.00
2019	1.58	1.37	0.68	21.45	28.24	11.92	4.84	340.88	1.93	802.51	0.97
2020	0.80	1.08	0.73	24.42	45.19	10.21	24.80	367.87	1.78	775.45	0.76
2021	0.70	0.11	0.15	19.32	49.15	7.34	24.95	399.56	1.63	837.89	0.50
2022	0.71	0.05	0.01	16.64	49.04	4.99	24.83	456.03	1.54	839.32	0.22

Table S4. Energy activity levels from the residential sector in Chengdu, as reported in the Chengdu Statistical Yearbook from 2010 to 2022.

Year \ Fuel Type	Liquefied Petroleum Gas (10,000 t)	Natural Gas (100 million m^3)
2010	4.92	6.68
2011	4.93	7.18
2012	5.08	7.60
2013	5.13	8.51
2014	4.96	8.56
2015	4.83	9.91
2016	4.71	13.01
2017	5.52	13.74
2018	5.17	16.02
2019	5.36	17.93
2020	5.19	17.81
2021	5.47	19.27
2022	4.67	20.60

Table S5. Vehicle Ownership by Type in Chengdu from 2010 to 2022.

Vehicle Type / Year	Private Cars (10,000 vehicles)	Buses (10,000 vehicles)	Taxis (10,000 vehicles)	Diesel Vehicles (10,000 vehicles)
2010	164.12	0.72	1.40	10.53
2011	192.82	0.72	1.24	11.40
2012	221.72	0.84	1.40	12.33
2013	258.90	1.32	1.49	13.71
2014	311.62	1.35	1.48	15.62
2015	365.48	1.41	1.40	17.36
2016	412.95	1.35	1.31	18.90
2017	432.45	1.44	1.20	20.01
2018	488.91	1.59	1.27	22.21
2019	516.74	1.59	1.65	23.38
2020	543.65	1.45	1.62	24.45
2021	573.00	1.67	1.69	25.59
2022	604.60	1.67	1.64	26.76

Table S6. Hourly $CO_{2,ff}$ concentrations in autumn.

Hour	0	1	2	3	4	5	6	7	8	9	10	11
$CO_{2,ff}$ (ppm)	15.14	13.20	12.62	11.81	13.59	15.98	16.84	18.49	20.15	20.88	21.69	22.70
Hour	12	13	14	15	16	17	18	19	20	21	22	23
$CO_{2,ff}$ (ppm)	24.13	22.76	21.52	19.36	19.00	18.09	18.91	19.82	19.45	17.00	15.91	15.27

Table S7. Seasonal averaged $CO_{2,ff}$ concentrations.

Season	Spring	Summer	Autumn	Winter
Ratio	0.96	0.97	1	1.22



Figure S1. DJI M600 Pro UAV sampling system equipped with an ABB LGR-ICOS GLA133 greenhouse gas analyzer. This instrument employs off-axis integrated cavity output spectroscopy (OA-ICOS) to provide high-precision, real-time CO_2 measurements with a sampling frequency of 1 Hz. The measurement precision is 0.35 ppm, expressed as one standard deviation (±1σ), enabling reliable high-resolution vertical profiling of greenhouse gas concentrations at urban and regional scales (see official documentation at https://search.abb.com/library/Download.aspx?DocumentID=DS%2FLGR-ICOS%2FGLA133-EN).

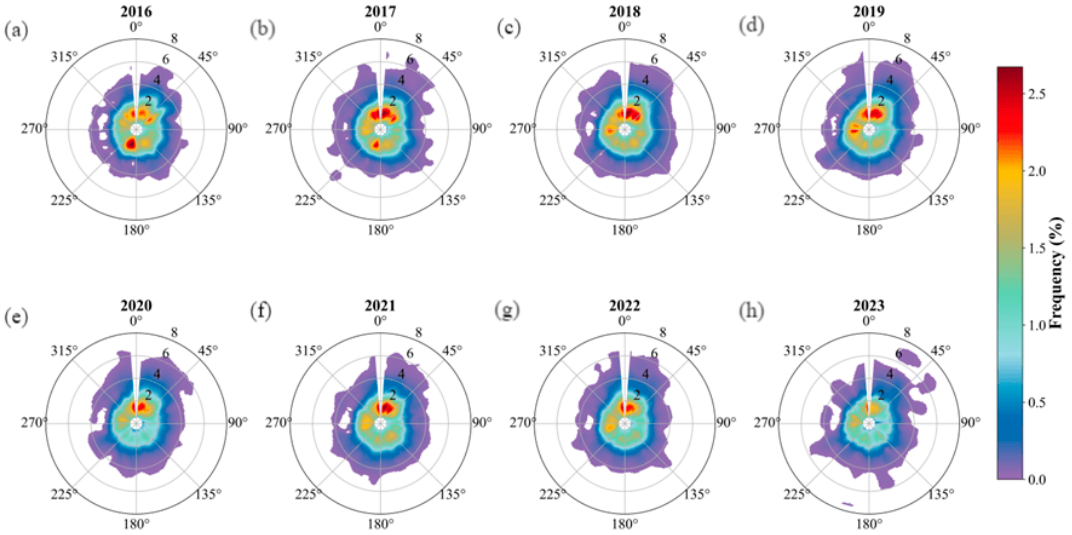


Figure S2. Wind Frequency Distribution in Chengdu from July to September (2016–2023) based on hourly wind direction data from the Wenjiang meteorological monitoring station.

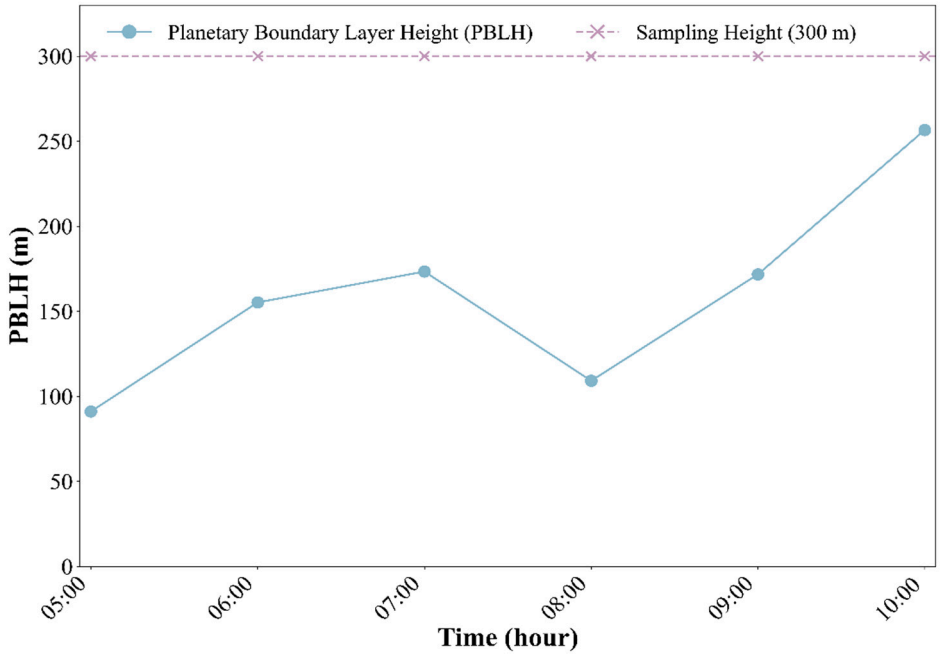


Figure S3. The planetary boundary layer heights of Chengdu during the sounding period.

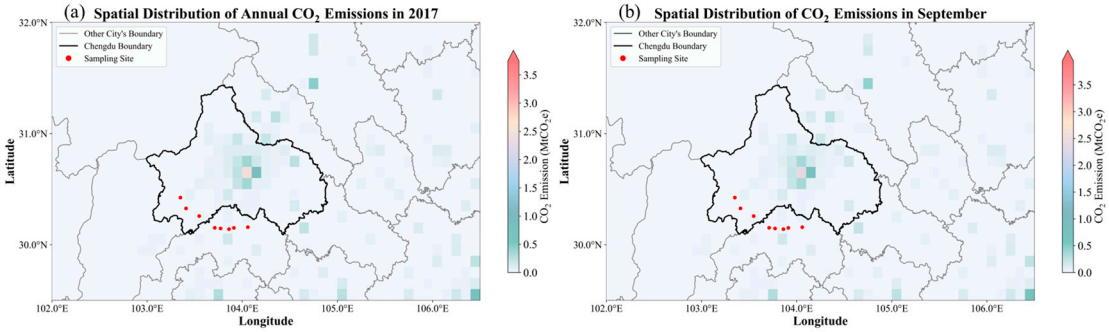


Figure S4. Spatial Distribution of (a) annual emissions and (b) emissions in September in 2017. The data were obtained from the MIXv2 dataset (available at http://meicmodel.org.cn/?page_id=2721, and accessed on 29th May, 2025).

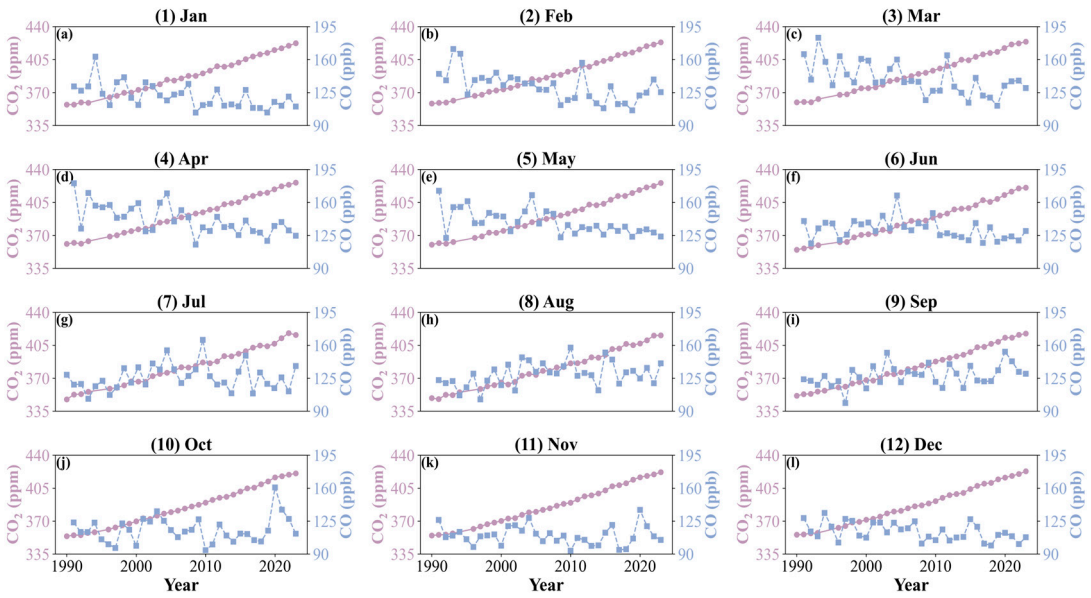


Figure S5. Monthly Trends of CO_2 and CO Concentrations at Waliguan Station from 1990 to 2023.

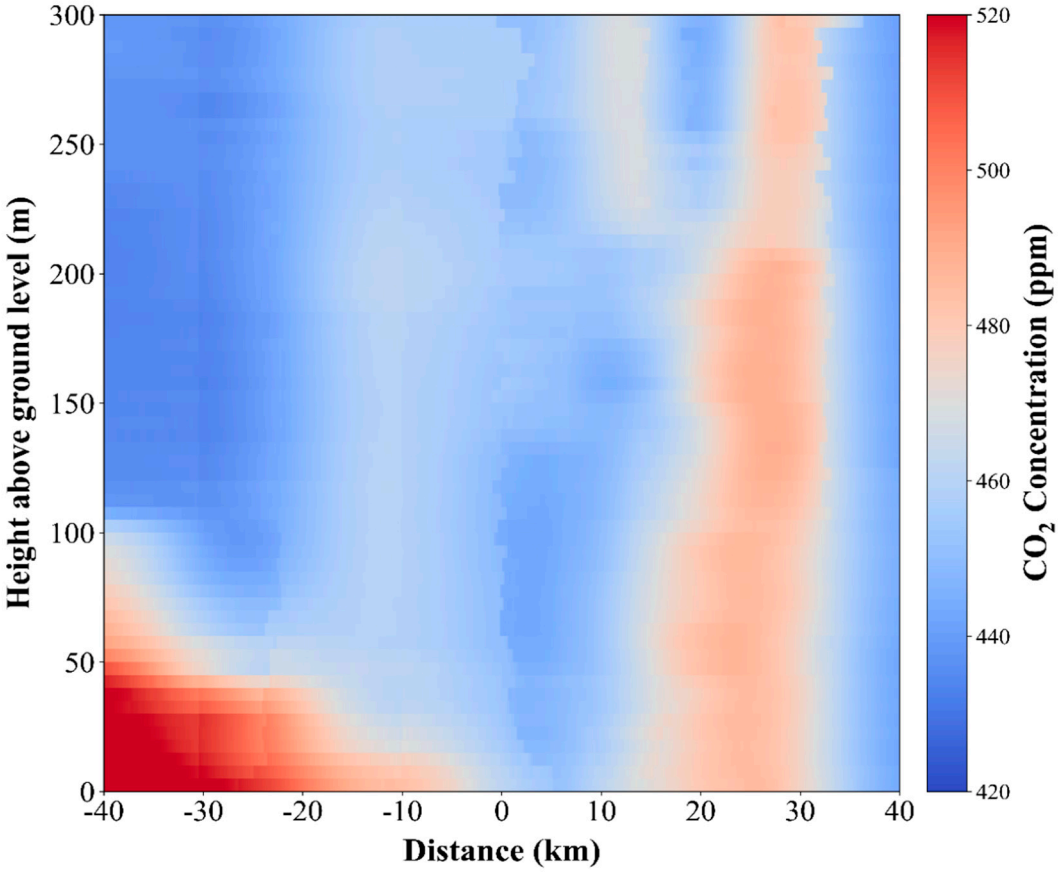


Figure S6. Kriging interpolation results showing the distribution of CO_2 concentrations. The horizontal axis represents the distance from the midpoint of the observation trajectory, with a negative value on the west side and a positive value on the east side.

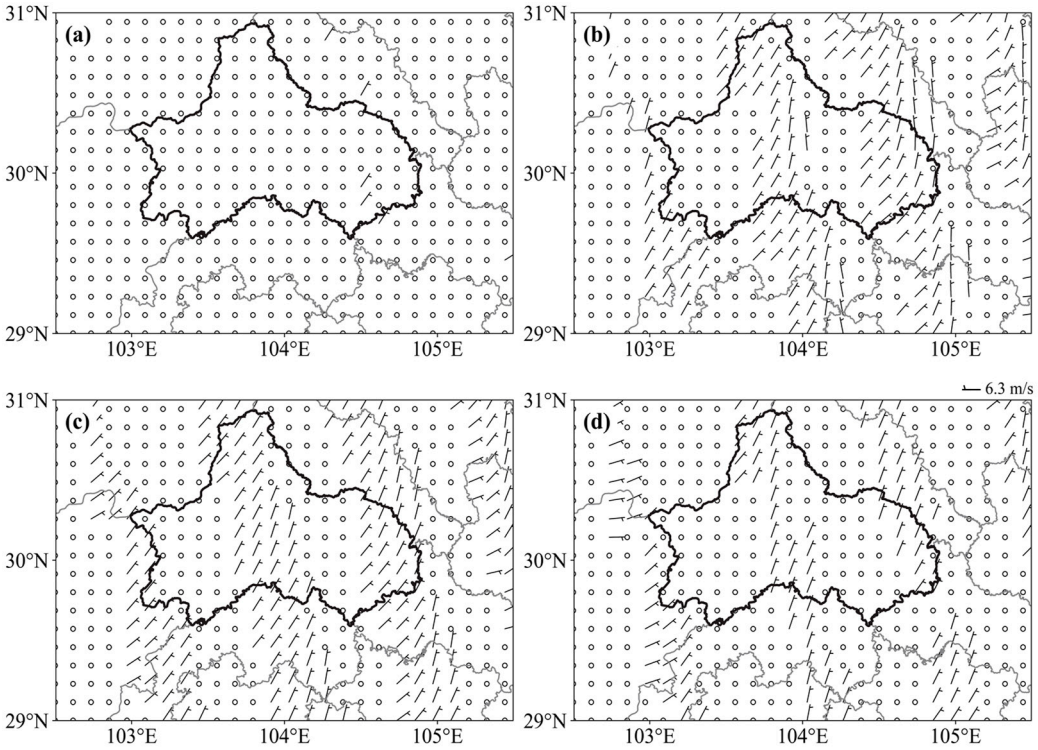


Figure S7. Wind field distributions over Chengdu at 975 hPa (a), 950 hPa (b), 925 hPa (c), and 900 hPa (d) at 5:00 a.m. on September 23, with the black outline indicating the administrative boundary of Chengdu.

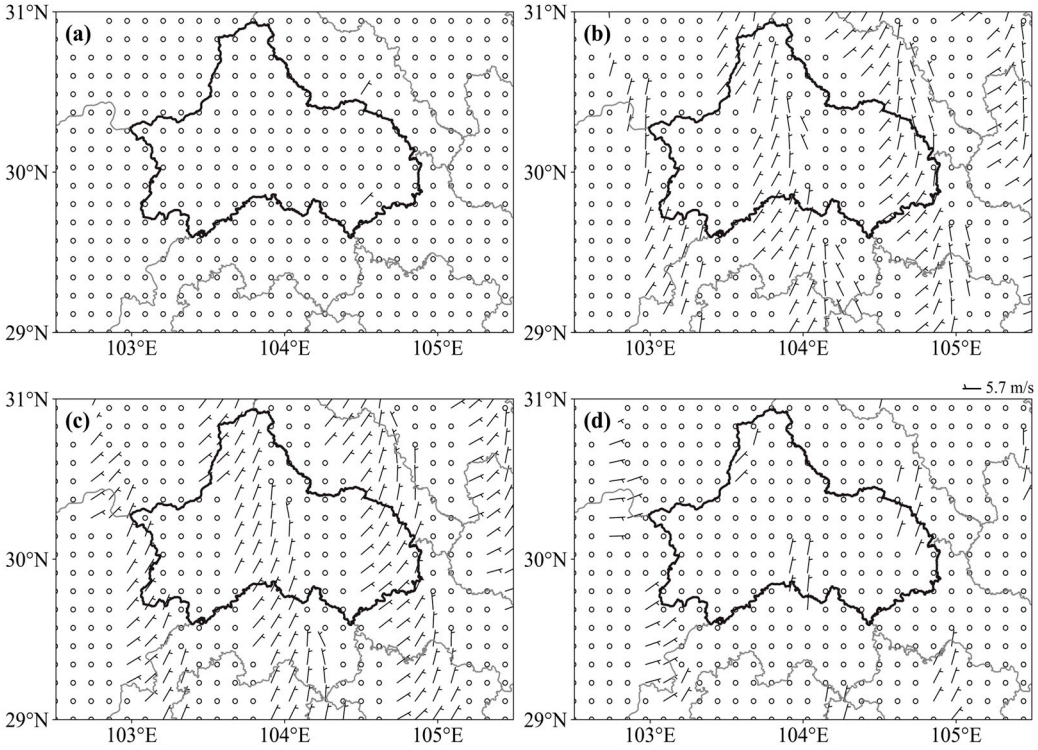


Figure S8. Wind field distributions over Chengdu at 975 hPa (a), 950 hPa (b), 925 hPa (c), and 900 hPa (d) at 6:00 a.m. on September 23, with the black outline indicating the administrative boundary of Chengdu.

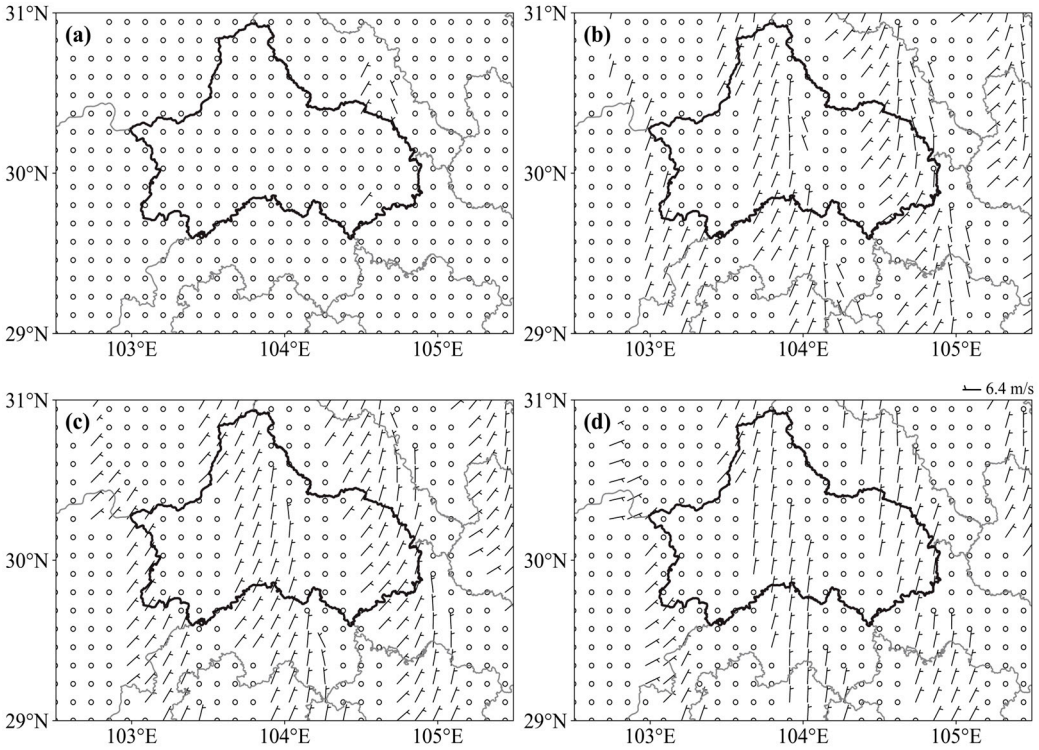


Figure S9. Wind field distributions over Chengdu at 975 hPa (a), 950 hPa (b), 925 hPa (c), and 900 hPa (d) at 7:00 a.m. on September 23, with the black outline indicating the administrative boundary of Chengdu.

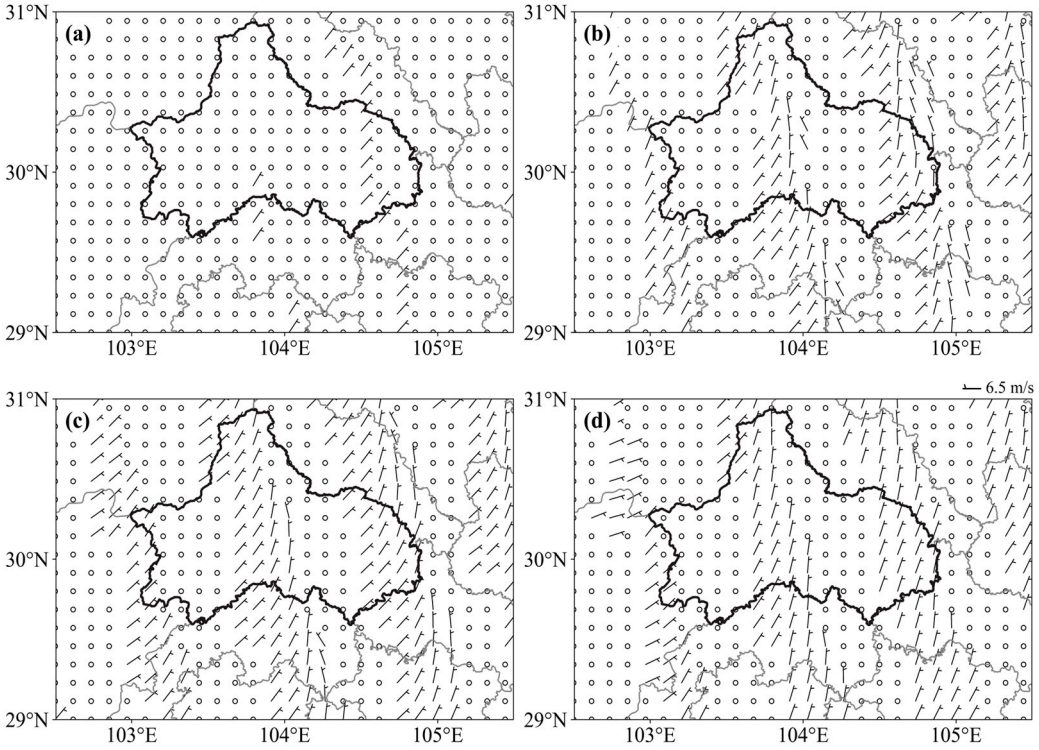


Figure S10. Wind field distributions over Chengdu at 975 hPa (a), 950 hPa (b), 925 hPa (c), and 900 hPa (d) at 8:00 a.m. on September 23, with the black outline indicating the administrative boundary of Chengdu.

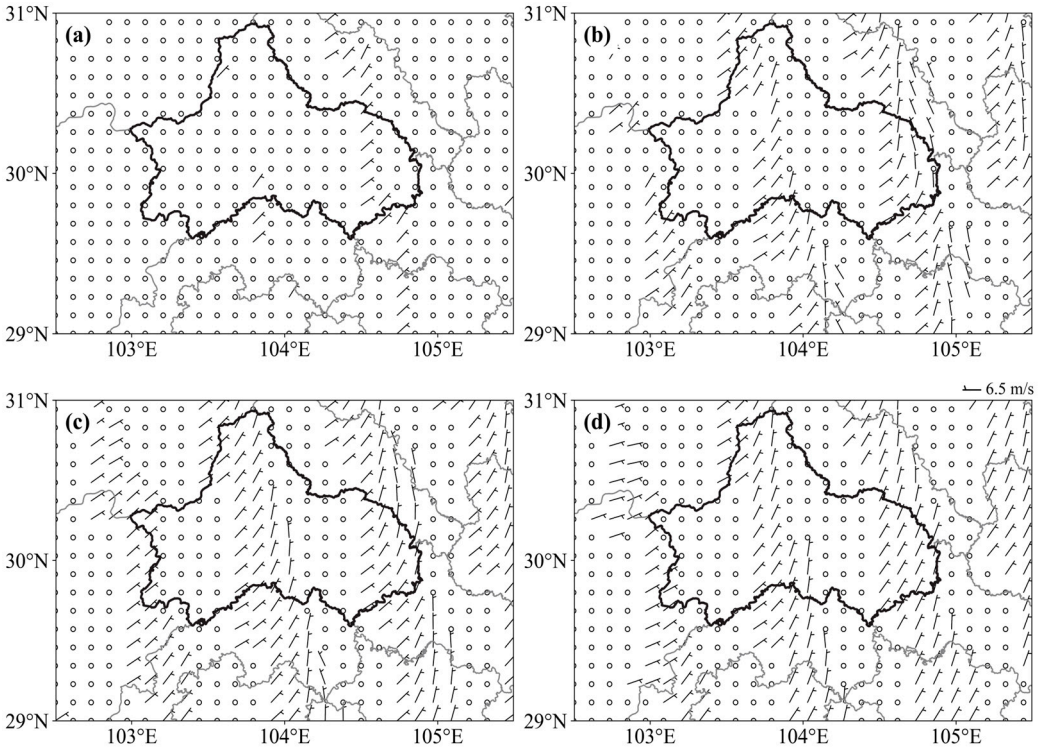


Figure S11. Wind field distributions over Chengdu at 975 hPa (a), 950 hPa (b), 925 hPa (c), and 900 hPa (d) at 9:00 a.m. on September 23, with the black outline indicating the administrative boundary of Chengdu.

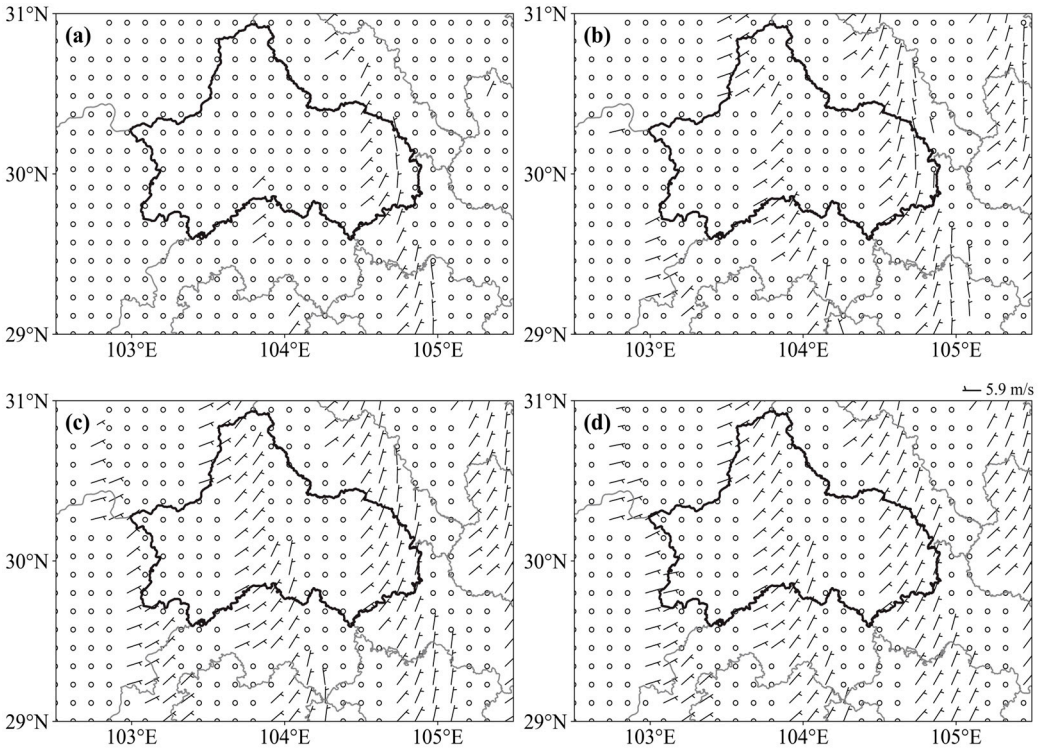


Figure S12. Wind field distributions over Chengdu at 975 hPa (a), 950 hPa (b), 925 hPa (c), and 900 hPa (d) at 10:00 a.m. on September 23, with the black outline indicating the administrative boundary of Chengdu.

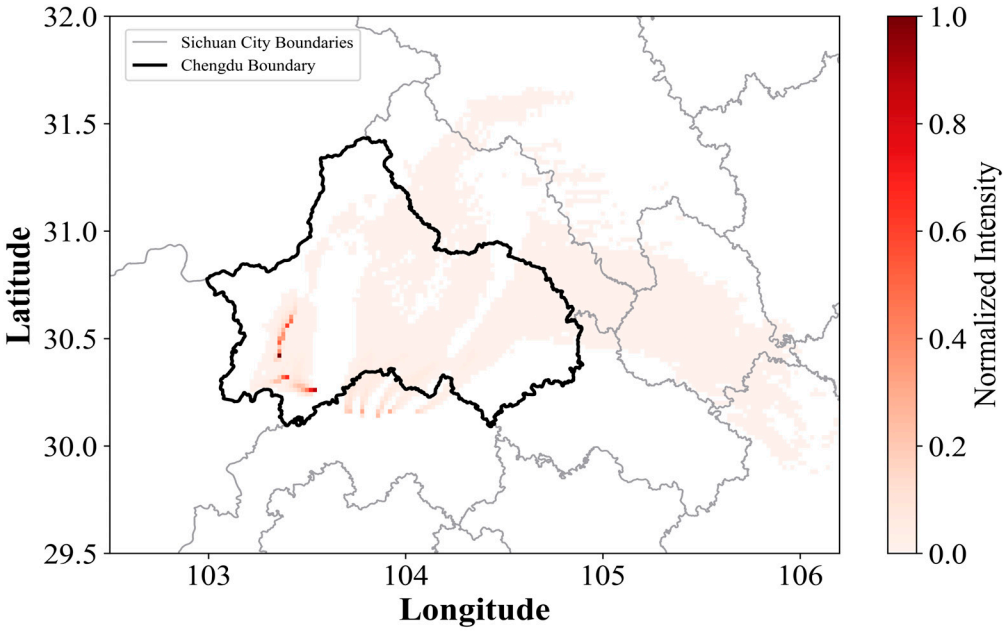


Figure S13. Spatial distribution of normalized 24-hour footprints at 5 m above ground level. The normalization was carried out by dividing the residence time at each grid by the maximum residence time within the research domain.

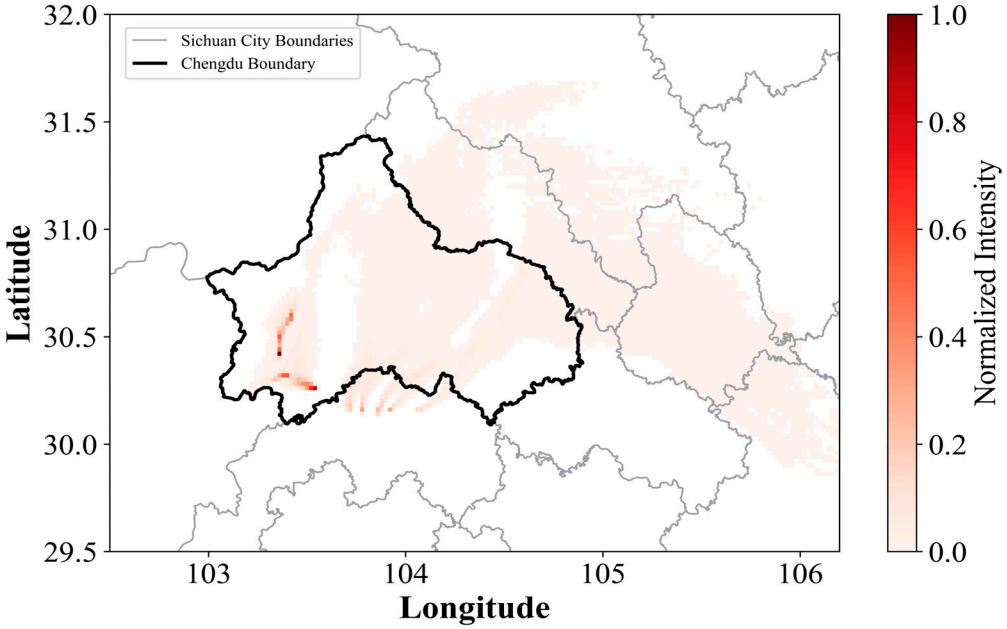


Figure S14. Spatial distribution of normalized 24-hour footprints at 100 m above ground level. The normalization was carried out by dividing the residence time at each grid by the maximum residence time within the research domain.

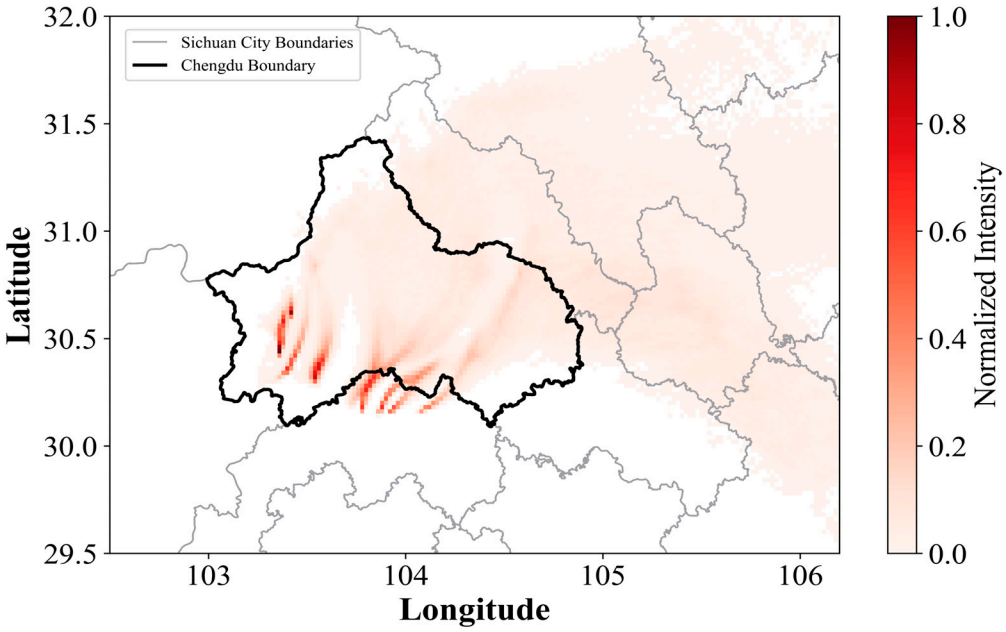


Figure S15. Spatial distribution of normalized 24-hour footprints at 200 m above ground level. The normalization was carried out by dividing the residence time at each grid by the maximum residence time within the research domain.

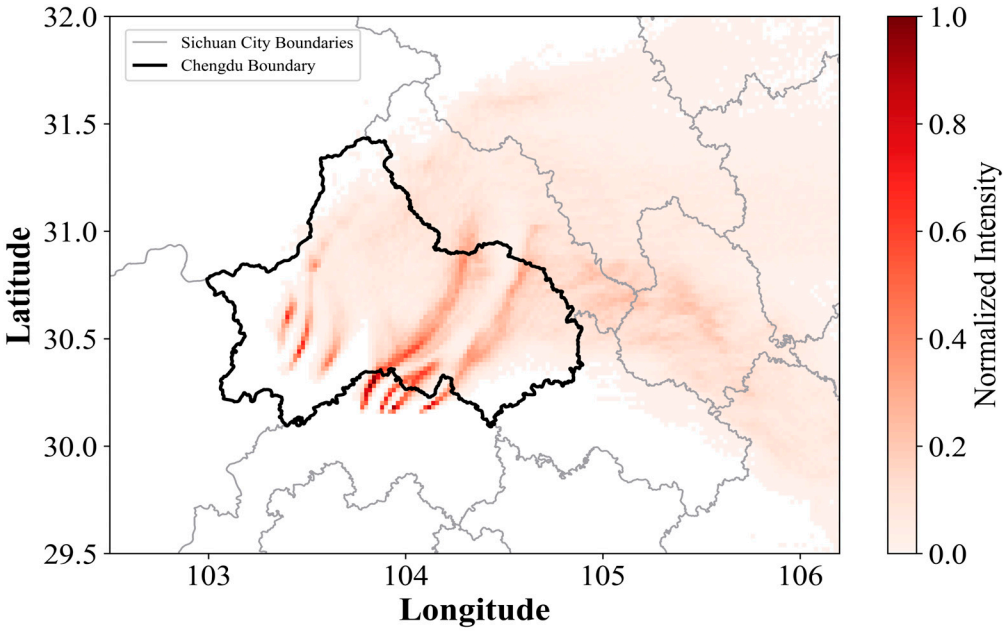


Figure S16. Spatial distribution of normalized 24-hour footprints at 300 m above ground level. The normalization was carried out by dividing the residence time at each grid by the maximum residence time within the research domain.

Reference

1. IPCC. 2019 Refinement to the 2006 IPCC Guidelines for National Greenhouse Gas Inventories; IPCC: Geneva, Switzerland, 2019; Available online: https://www.ipcc.ch/report/2019-refinement-to-the-2006-ipcc-guidelines-for-national-greenhouse-gas-inventories/ (accessed on 6 February 2025).